Influence of Microstructure on Crack-Tip Micromechanics and Fracture Behaviors of a Two-Phase TiAl Alloy

K.S. CHAN and Y.-W. KIM

The tensile deformation, crack-tip micromechanics, and fracture behaviors of a two-phase (γ + α_2) gamma titanium aluminide alloy, Ti-47Al-2.6Nb-2(Cr + V), heat-treated for the microstructure of either fine duplex (gamma + lamellar) or predominantly lamellar microstructure were studied in the 25 °C to 800 °C range. *In situ* tensile and fracture toughness tests were performed in vacuum using a high-temperature loading stage in a scanning electron microscope (SEM), while conventional tensile tests were performed in air. The results revealed strong influences of microstructure on the crack-tip deformation, quasi-static crack growth, and the fracture initiation behaviors in the alloy. Intergranular fracture and cleavage were the dominant fracture mechanisms in the duplex microstructure material, whose fracture remained brittle at temperatures up to 600 °C. In contrast, the nearly fully lamellar microstructure resulted in a relatively high crack growth resistance in the 25 °C to 800 °C range, with interface delamination, translamellar fracture, and decohesion of colony boundaries being the main fracture processes. The higher fracture resistance exhibited by the lamellar microstructure can be attributed, at least partly, to toughening by shear ligaments formed as the result of mismatched crack planes in the process zone.

I. INTRODUCTION

TITANIUM aluminide alloys based on gamma TiAl are of interest as a potentially important aerospace structural material because of their light weight, relatively good high-temperature mechanical properties, and oxidation resistance.[1-4] Unfortunately, neither the ductility nor the fracture toughness of these TiAl-alloys is particularly high at ambient temperature. Coupled with poor formability, the TiAl-alloys are still far from being fully utilized in aerospace applications. With alloy modification and microstructure control, however, both ductility[3,5] and toughness[5,6] have been improved significantly in two-phase gamma titanium aluminide alloys during the last couple of years, although these alloys are still not adequate for application.

Advanced two-phase TiAl-alloys generally consist of Ti-(46 to 49) at. pct Al-(2 to 5) at. pct M, M being at least one element from V, Cr, Mn, and Nb, with occasionally W or Mo.[3,7-10] In the as-cast conditions,[3,11] or when heat-treated in the α phase field,[3,6,7,12] the two-phase TiAl-alloys exhibit a lamellar microstructure consisting of alternating layers of ordered γ ($L1_0$ structure) and α_2 ($D0_{19}$ structure) platelets. Duplex microstructures consisting of equiaxed gamma grains with small amounts of alpha-2 in plate or particulate forms can be formed when heat treated in the (α + γ) phase field.[3,6,7,13] Both the amount of alpha$_2$ phase and the relative volume fraction of lamellar and equiaxed γ grains are important factors controlling the fracture properties of two-phase TiAl-alloys.[2,4,8] Maximum tensile ductility was obtained in a two-phase TiAl-alloy containing approximately 10 vol pct of the α_2 phase.[8] The best balance of properties with good elevated-temperature creep resistance and acceptable tensile strength and ductility in current two-phase TiAl-alloys appears to occur at about 30 vol pct of lamellar grains and 70 vol pct equiaxed grains.[3,7,14]

While these previous results clearly indicate the beneficial effects of the lamellar microstructure, the mechanisms by which the aligned microstructure imparts fracture toughness and tensile ductility remain unclear. It has been suggested that the lamellar microstructure enhances the ductility in Ti-48Al by inducing fine, uniform deformation of γ plates in the early stage of deformation and then α_2 plates in the latter stage.[9] The activation of twinning in the lamellar microstructure may also be an important, beneficial factor for improving the fracture characteristics of the two-phase γ alloy.[1]

The objective of this article is to present the results of an investigation aimed at studying the effect of microstructure on the fracture processes and crack growth resistance in two-phase TiAl-alloys. In particular, the fracture mechanisms that occur within the crack-tip process zone will be examined for both duplex and lamellar microstructures at ambient and elevated temperatures. The results will then be used to define microstructure/property relationships in two-phase TiAl-alloys. Some of the results on fracture mechanisms at ambient temperature that have been reported earlier[15] are included here so that relationships between fracture mechanism, tensile ductility, and crack growth resistance can be elucidated.

II. EXPERIMENTAL PROCEDURES

A gamma titanium aluminide alloy designed as G1 was prepared at Duriron using skull-melting and casting techniques[16] into a 6.9-cm-diameter × 80-cm-long ingot

K.S. CHAN, Principal Engineer, is with the Department of Materials and Mechanics, Southwest Research Institute, San Antonio, TX, 78238-5166. Y.-W. KIM, Group Leader, is with the Metcut-Materials Research Group, Wright-Patterson AFB, OH 45433-0511.

Manuscript submitted September 3, 1991.

Table I. Heat-Treatment Procedures, Microstructures, and Tensile and Fracture Properties of the Near-Gamma Alloy Ti-47Al-2.6Nb-2(Cr + V)*

Material*	Heat Treatment	Microstructure	T, °C	σ_y, NPa	σ_{UTS}, MPa	N	Total Elongation, Pct	K_{IC}, MPa$\sqrt{m}$	T_R	K_s,** MPa$\sqrt{m}$
G1F	1275 °C/3 h in vacuum/ controlled cool to 900 °C	duplex microstructure predominantly equiaxed γ plus small amounts of α_2 particles and plates	25	415.6	557.9	0.09/0.036	3.7	11.4	0	11.4
			600	342.0	600.5	0.11/0.039	7.3	16.1	0	16.1
	aging at 900 °C/4 h/ FC in vacuum		790	168.4	295.9	0.136	13.0	—	—	—
G1L	1360 °C/1 h in vacuum/ controlled cool to 900 °C	nearly fully-lamellar microstructure predominantly lamellar $\alpha_2 + \gamma$ microstructure plus small amounts of equiaxed γ grains at colony boundaries	25	329.6	383.1	0.162	0.88	16.0	≈ 0.94	25.0
	aging at 900 °C/6 h/ AC†		800	289.4	377.6	0.156	1.50	35.0	102.0	>61.0

*Materials supplied by Metcut-Materials Research Group at Wright-Patterson AFB.
**Asymptotic or maximum value of stress intensity factor in the K-resistance curve.
†FC = furnace cooled.
‡AC = air cooled.

weighing roughly 21 kg. The alloy composition determined by both wet chemical analyses and atomic absorption techniques was Ti-47.0Al-2.6Nb-.093Cr-0.85V (in atomic percent), with impurity levels of 550 oxygen, 55 nitrogen, 160 carbon, and 14 hydrogen in weight parts per million. A 10-cm-long billet was sectioned from the ingot, which was subsequently hot isostatically pressed at 1150 °C under 276 MPa pressure for 3 hours. The billet was then forged into a 2-cm-thick × 15-cm-diameter pancake in a 980 °C hot die after soaking at 1200 °C for 2 hours.[17]

Two sample pieces, G1F and G1L, were sectioned from the pancake and given two different heat treatments to generate entirely different microstructures (Table I). The sample G1F contained a duplex microstructure consisting of predominantly fine equiaxed gamma grains approximately 40 μm in diameter and small amounts of α_2 particles and plates located at grain boundaries (Figures 1(a) and 1(c)). The microstructure of G1L was nearly fully lamellar, consisting of large lamellar colonies (*i.e.*, grains) approximately 1.6 mm in diameter and small amounts of fine grain boundary gamma grains (Figure 1(b)). The lamellar structure is alternating layers of γ/α_2 platelets, as shown in the backscattered electron image in Figure 1(d). The gamma plates and α_2 plates in the lamellar structure had the crystallographic orientation relationship of $(111)_\gamma // (0001)_{\alpha_2}$ and $[110]_\gamma // [2110]_{\alpha_2}$, which is consistent with previous observations.[3,6,11,12]

Tensile and fracture toughness tests were performed on both the duplex and lamellar microstructures at 25 °C, 600 °C, and 800 °C. Two different types of round-bar tensile specimens were used for testing conventionally in air and for *in situ* testing in vacuum, respectively. The conventional tensile specimens were 17 mm in gage length, 3.2 mm in diameter at the gage section, and 48 mm in total length. The *in situ* tensile specimens were 13.5 mm in gage length, 2 mm in diameter at the gage section, and 54 mm in total length. The fracture toughness specimens were of the single-edge-notched (SEN) geometry whose dimensions were reported earlier.[18] After machining, tensile and SEN specimens were mechanically polished and then electropolished using a solution of 5 pct H_2SO_4 in methanol maintained at −40 °C. The SEN specimens were subsequently fatigue-precracked and ion-milled to enhance the visibility of the microstructural features in a scanning electron microscope (SEM).

Conventional tensile tests were conducted in air using a servohydraulic testing machine equipped with a clamshell furnace. The imposed strain rate was 1×10^{-3} s^{-1}. Strains were measured *via* a high-temperature extensometer attached to the shoulder sections of the test specimens. Both the *in situ* tensile and fracture toughness tests were performed at a vacuum of 1.3×10^{-3} Pa or better in an SEM equipped with a loading stage whose temperature capacity is ≈800 °C.[19] During *in situ* tensile and fracture toughness testing, still photographs of the gage section or the crack-tip region were obtained as a

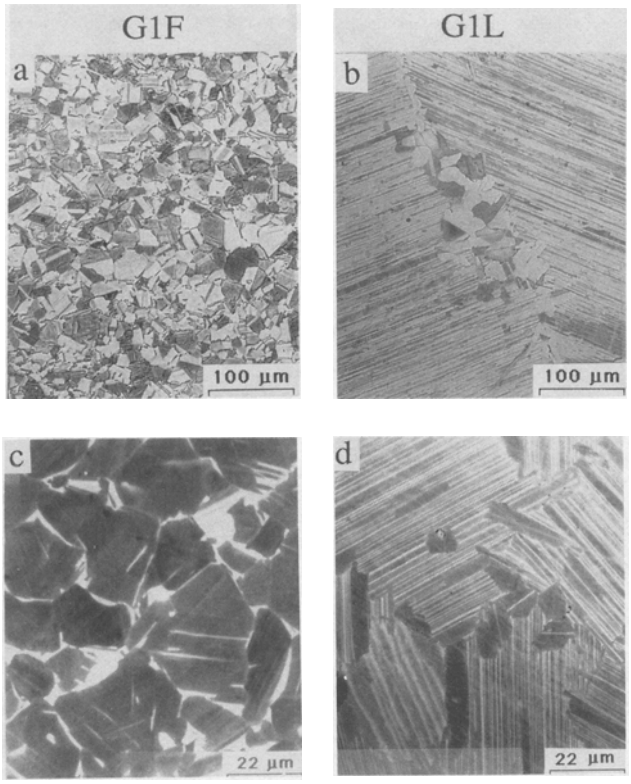

Fig. 1—Microstructures of (*a*) and (*c*) G1F and (*b*) and (*d*) G1L showing: fine gamma grains in optical micrograph (a) with grain boundary α_2 phases imaged bright in the backscattered electron image (c); large lamellar grains (b) consisting of alternative layers of gamma plates and α_2 plates (d) with fine grain boundary gamma. The α_2 plates in the lamellar structure are imaged light in the backscattered electron image (d).

function of loads or stress intensity, K, levels. Photographs of the loaded and unloaded cracks were subsequently analyzed using a machine-vision-based stereo-imaging technique[20,21] to obtain the displacement of materials points near the crack-tip region. The near-tip strain components were then computed in terms of the displacements gradients using procedures described earlier.[22] The fracture surfaces of the tensile and fracture toughness specimens were also examined using scanning electron microscopy.

III. RESULTS

A. *Tensile Behavior*

Engineering stress-strain curves of the Ti-47Al-2.6Nb-2(V +Cr) alloy tested in air are shown in Figures 2(a) and (b) for the duplex microstructure and the lamellar microstructure, respectively. The duplex microstructure has been found to exhibit a higher yield stress, ultimate tensile strength, and total elongation than the lamellar microstructure at ambient temperature, as summarized in Table I. The strength of the duplex microstructure, however, decreases with increasing temperature at a faster rate than the lamellar microstructure. At 800 °C, the yield and tensile strengths are higher in the lamellar microstructure than in the duplex microstructure. The total

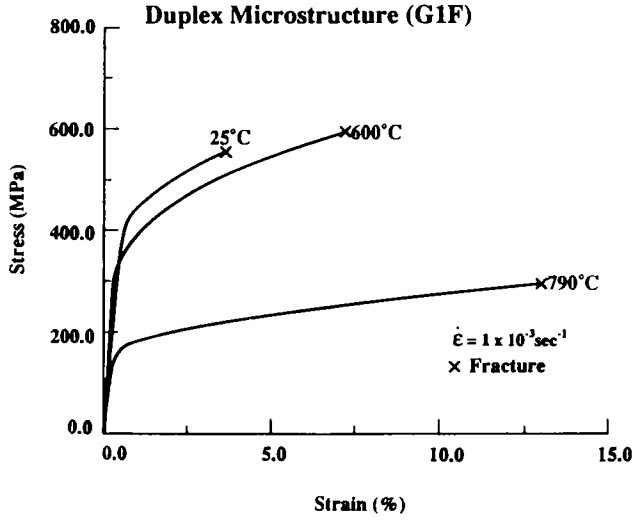

(*a*)

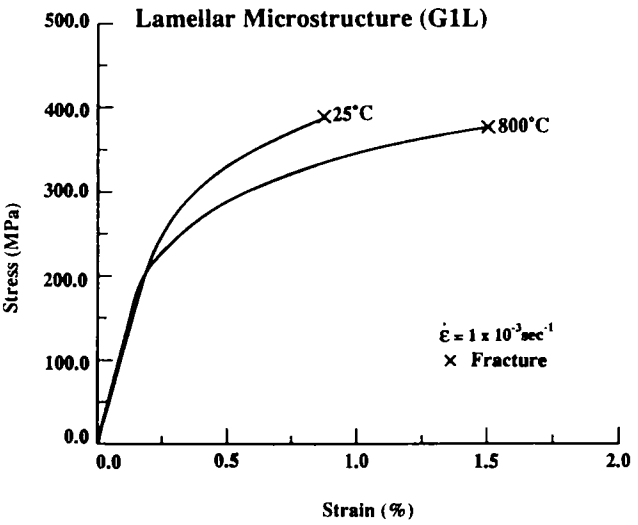

(*b*)

Fig. 2—Engineering stress-strain curves of Ti-47Al-2.6Nb-2(Cr +V): (*a*) duplex microstructure and (*b*) near-lamellar microstructure.

elongation of the duplex microstructure is 3.7 pct at 25 °C, and it increases with increasing temperature to approximately 13 pct at 790 °C. In contrast, the lamellar microstructure exhibits a total elongation of 0.88 pct at 25 °C, and it increases to 1.5 pct only at 800 °C. Substantial differences in the strain-hardening behavior have also been observed between the two microstructures. As illustrated by the true stress-true strain curves in Figure 3, the duplex microstructure shows higher strain hardening and larger values of the strain-hardening exponent, N, than the lamellar microstructure. The N value for the duplex microstructure increases with plastic strains. Initial and final (prior to fracture) values of N for this material are compared with those for the lamellar microstructure in Table I.

The lack of tensile ductility exhibited by the lamellar microstructure was studied using *in situ* tensile tests in the SEM loading stage at both 25 °C and 800 °C in a

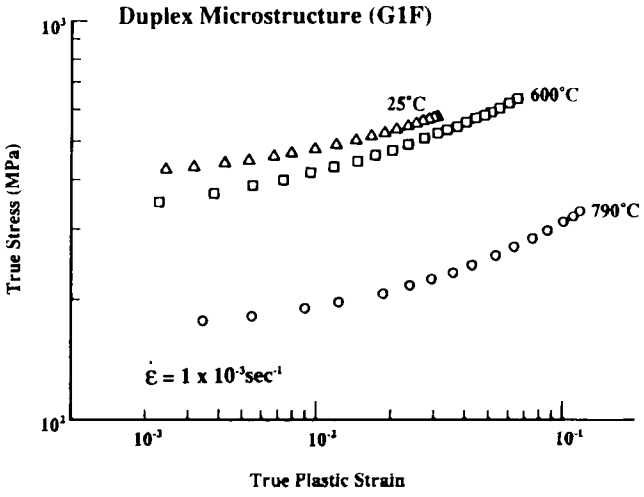

(*a*)

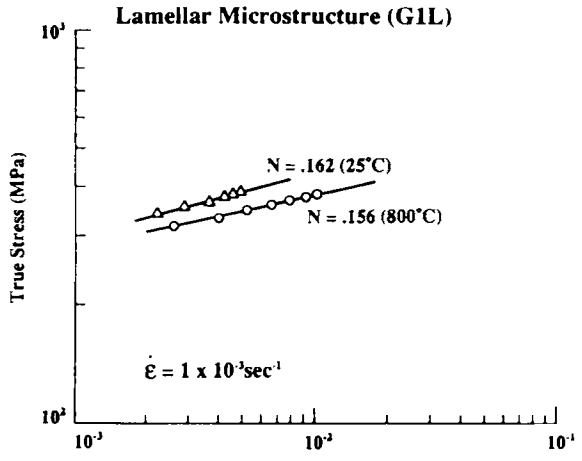

(*b*)

Fig. 3—True stress–true strain curves of Ti47Al-2.6Nb-2(Cr + V) in log-log plots: (*a*) duplex microstructure and (*b*) near-lamellar microstructure.

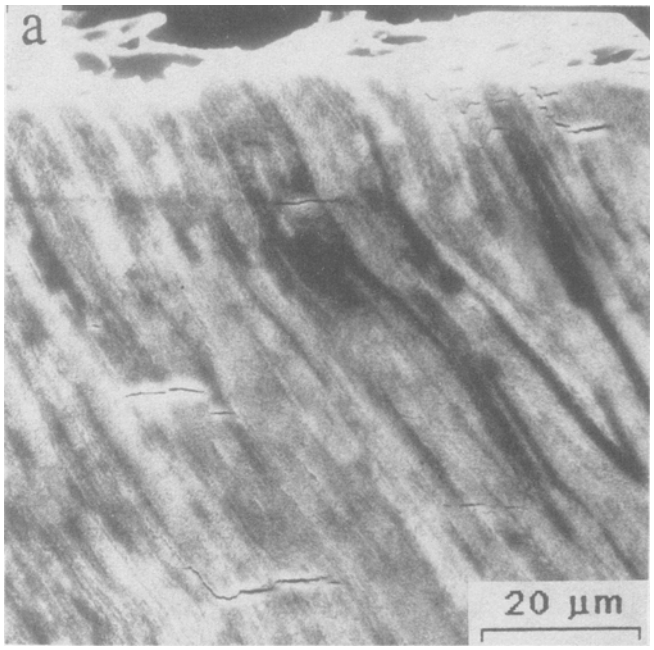

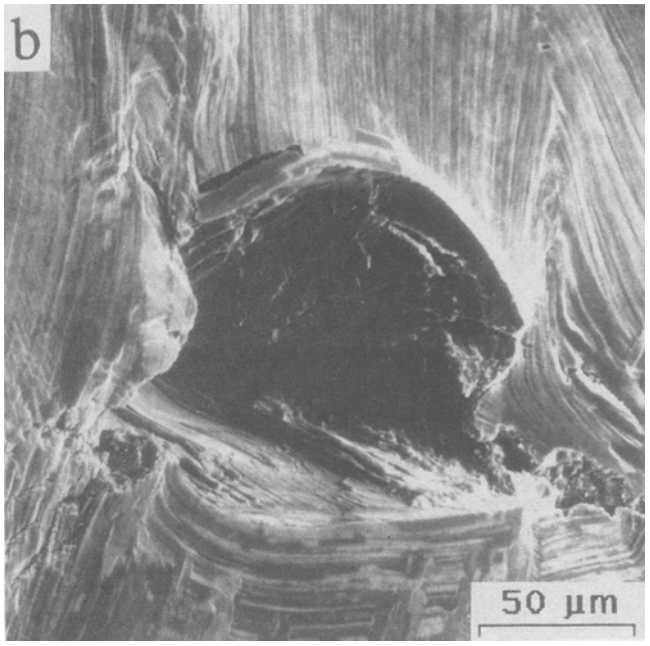

Fig. 4—Characteristics of microcracks observed in tensile specimens of the lamellar material (G1L): (*a*) tested at 25 °C and at $\dot{\varepsilon} = 1 \times 10^{-3}$ s^{-1} in air and (*b*) tested in vacuum at 800 °C at $\dot{\varepsilon} \approx 1 \times 10^{-5}$ s.

vacuum better than 1.3×10^{-3} Pa. During the tensile test, the load was incrementally increased and stopped periodically so that the gage section of the tensile specimen could be photographed. At 25 °C, the near lamellar microstructure remained brittle and exhibited low ductility (ε_{1f} = 0.75 pct) in vacuum. There were no significant differences between the reduction in area and fracture strains in air and in vacuum. Examining the fractured specimen revealed small microcracks along the gage section of the specimen, as shown in Figure 4(a), suggesting that tensile fracture appeared to be controlled by initiation of microcracks. In contrast, tensile fracture of the lamellar microstructure at 800 °C in vacuum was controlled by crack propagation. Figure 4(b) shows a relatively large microcrack formed at lamellar colony boundaries. Resistance to crack propagation was so large that the load capacity of the loading stage was exceeded prior to fracture of the specimen. Many microcracks and crack initiation sites were observed in the lamellar microstructure, including boundaries of (1) equiaxed γ grains (Figure 5(a)), (2) lamellar colonies (Figure 5(b)), (3) equiaxed γ grain and lamellar colonies (Figure 5(c) and (d)), and (4) lamellar interfaces (indicated by arrows in Figure 5(c)).

Results of an *in situ* tensile test at 800 °C for G1F revealed microcrack initiation mostly at grain boundaries, with the microcrack formation process being quite similar to those associated with the equiaxed grains in the G1L material shown in Figure 6. At 800 °C, the equiaxed gamma grains in the G1F alloy and the G1L

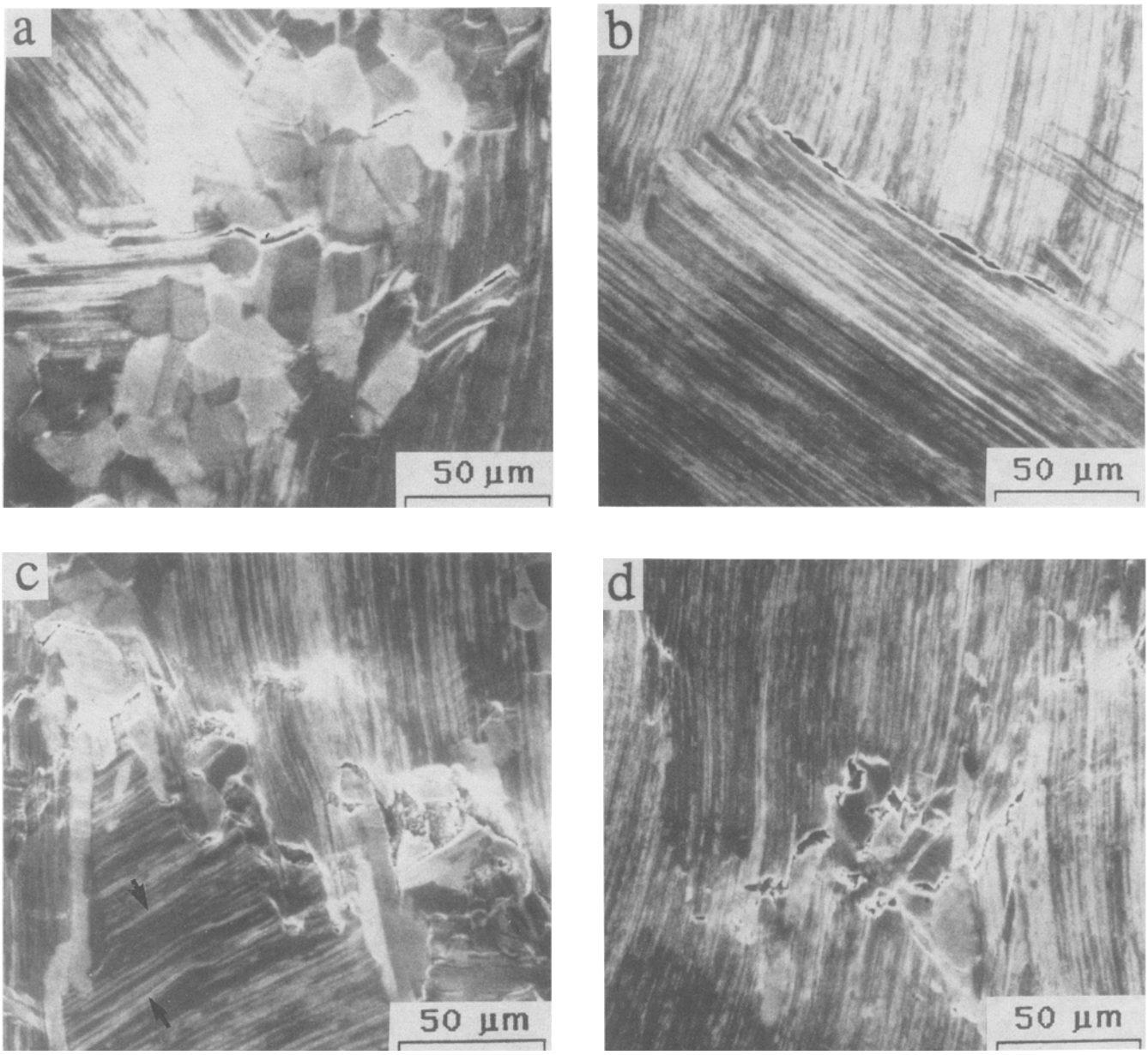

Fig. 5—Crack initiation sites in the lamellar (L) microstructure: (*a*) equiaxed γ grain boundaries, (*b*) lamellar colony boundary, (*c*) lamellar interfaces, γ grains, and γ/L interfaces, and (*d*) γ/L interfaces.

alloy were sufficiently ductile that the microcracks, once nucleated, did not propagate unstably but exhibited blunting and crack opening, upon increasing loads, as shown in Figure 6. Additional microcracks were initiated upon continued loading (Figure 6(c)). Final fracture eventually occurred in the G1F material when the microcracks linked to form a macrocrack of a critical length. In the case of the G1L alloy, fracture was dominated by the lamellar grains.

Comparisons of the stress–strain curves for the G1L material in air and in vacuum are shown in Figure 7(a) for 25 °C and Figure 7(b) for 800 °C, respectively. The strain rate for the testing at 25 °C was $\approx 1 \times 10^{-3}$ s^{-1}. For the 800 °C testing, the strain rate was 1×10^{-3} s^{-1} for the specimen tested in air but was $\approx 1 \times 10^{-5}$ s^{-1} for the specimen tested in vacuum. At 25 °C, the G1L material exhibited essentially identical stress–strain behavior, including tensile ductility in air and in vacuum (Figure 7(a)). In contrast, the material showed much higher ductility and ultimate tensile strength in vacuum than in air at 800 °C, with the yield stress not significantly affected by the test environment. This finding suggests that the low tensile ductility observed in air at 800 °C might be either an environmental embrittlement effect or a strain-rate effect.

B. *Fracture Behavior*

Despite lower ductility, the lamellar microstructure (G1L) has been found to exhibit higher fracture resistance than the duplex microstructure (G1F) at 25 °C. This is illustrated by the *K*-resistance curves shown in

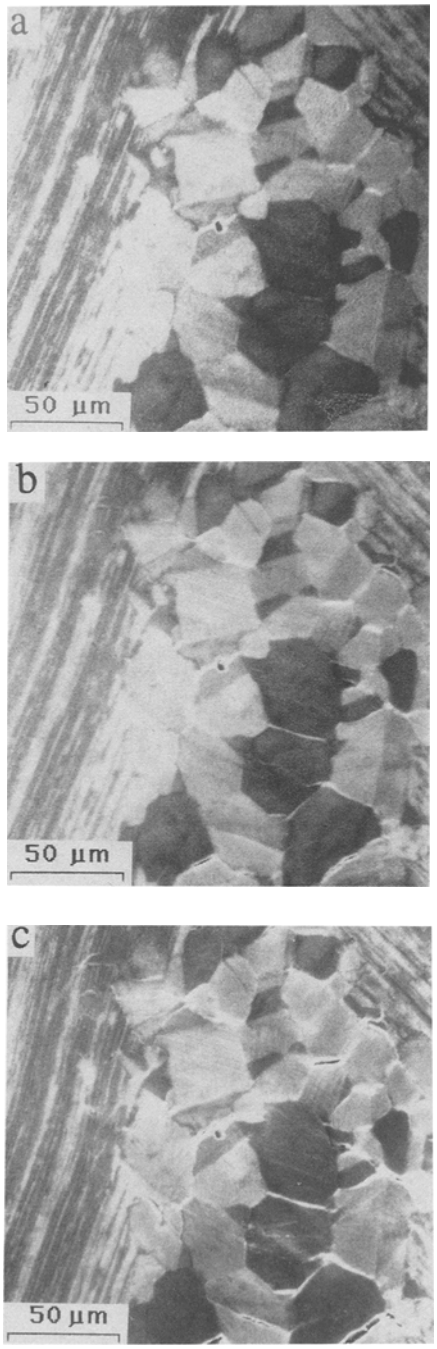

Fig. 6—Microcrack initiation and coalescence processes at equiaxed γ grains upon increasing levels in the near-lamellar (G1L) material: (*a*) 420 MPa, (*b*) 520 MPa, and (*c*) 570 MPa.

Figure 8. The fracture toughness results, which are summarized in Table I, demonstrate that G1L exhibits higher initiation toughness (K_{IC} value), as well as crack growth toughness, than the G1F material. The K_{IC} value for the duplex microstructure ranges from 10 to 16 MPa$\sqrt{\text{m}}$, with a zero value of tearing modulus, T_R ($T_R = E/\sigma_0^2\, dJ/da$, where E is Young's modulus, σ_0 is the flow stress, and dJ/da is the initial slope of the J-resistance curve), at 25 °C and 600 °C. In contrast, the K_{IC} value for the lamellar microstructure increases from 16 to 36 MPa$\sqrt{\text{m}}$, and the tearing modulus, T_R, increases from

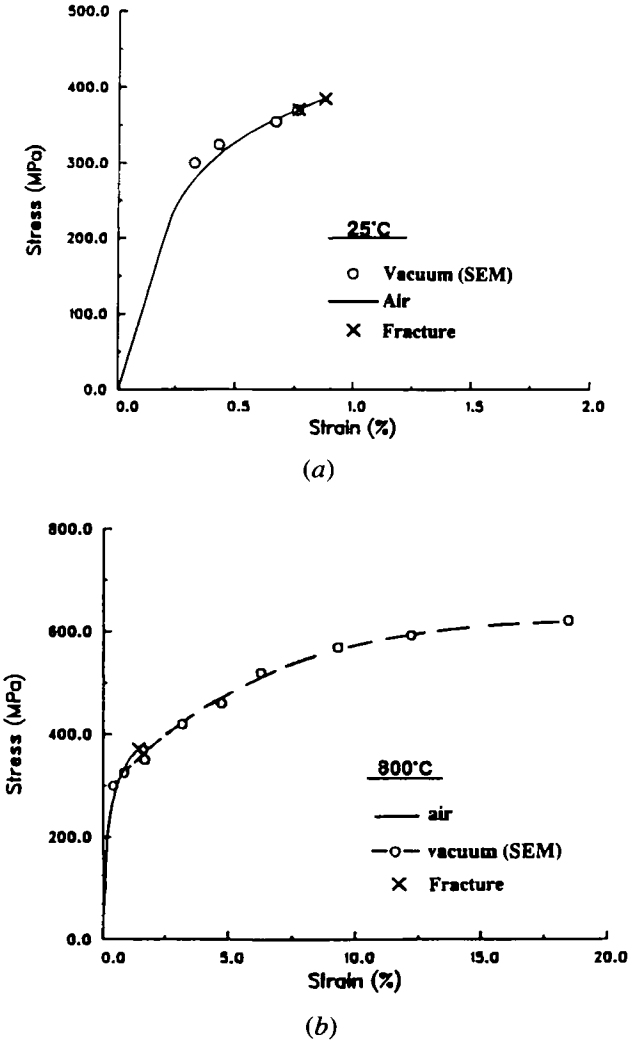

Fig. 7—Comparison of stress-strain curves of the G1L alloy, lamellar Ti-47Al-2.6Nb-2(Cr,V), tested in air and in vacuum: (*a*) 25 °C, $\dot{\epsilon} \approx 1 \times 10^{-3}$ s^{-1} for both in air and vacuum and (*b*) 800 °C, $\dot{\epsilon} = 1 \times 10^{-3}$ in air and $\dot{\epsilon} = 1 \times 10^{-5}$ in vacuum.

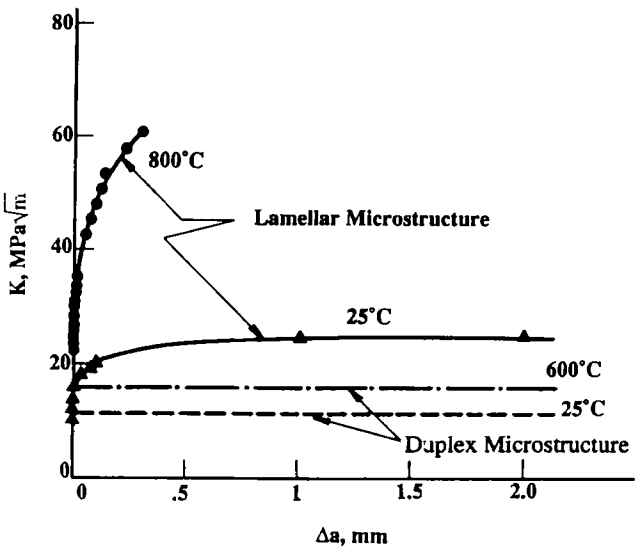

Fig. 8—K-resistance curves of the duplex (G1F) and the nearly fully lamellar (G1L) microstructures.

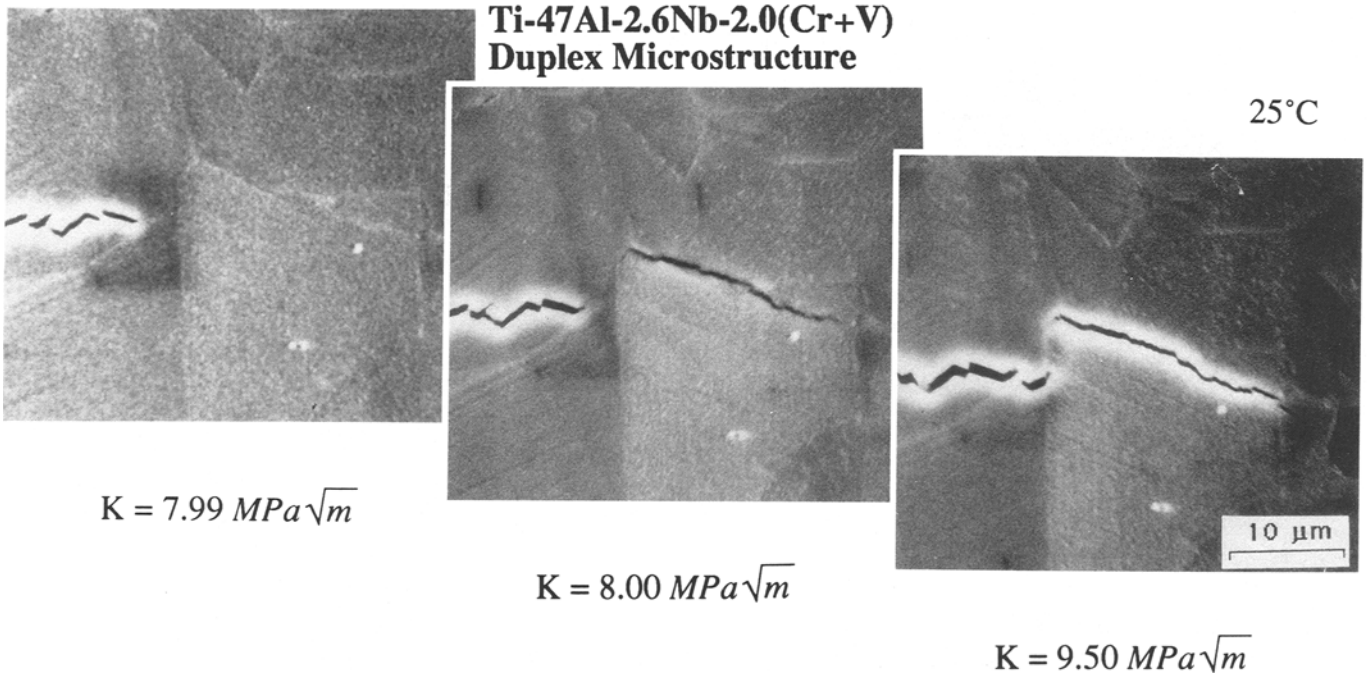

Fig. 9 — Near-tip fracture process in the duplex microstructure (G1F) at 25 °C.

≈0.94 to 102 when the temperature is raised from 25 °C to 800 °C.

The near-tip fracture mechanisms in the duplex microstructure (G1F) tested at 25 °C are summarized in Figure 9, which shows a grain boundary microcrack is initiated ahead of the main crack tip when the K level is raised to approximately 8 MPa$\sqrt{m}$. The planes of the microcrack and the main crack are unconnected, resulting in a shear ligament whose failure led to a complete fracture of the test specimen when the K level was raised above 11 MPa$\sqrt{m}$. The strain distribution in the process zone is shown in Figure 10(a), which shows that the strains within the near-tip equiaxed gamma grain that exhibits grain boundary decohesion are on the order of the yield strain (yield stress/Young's modulus). This observation indicates that the microcrack might have been induced as the result of plastic incompatibility at the grain boundary due to impinging slip developed in the equiaxed γ grains.

Figure 11 presents the near-tip fracture process in the nearly fully lamellar microstructure tested at ambient temperature, which exhibits the near-tip strain distribution shown in Figure 10(b). At K = 14 MPa $\sqrt{m}$, the crack was found to open with bifurcated tips, one of which lay along the α_2/γ interface. At K = 16 MPa$\sqrt{m}$, the main crack extended in a direction parallel to the γ and α_2 plates in the lamellae. Microcracks were nucleated along or across the lamellae located ahead of the crack tip. Further increase to K = 19 MPa $\sqrt{m}$ caused extension of the main crack, its linkage with the microcracks, larger crack opening displacement, and generation of additional microcracks ahead of the crack tip. The microcracks and the main crack were connected by ligaments that were formed between the mismatched crack planes. At K = 21 MPa$\sqrt{m}$, extensive microcracking was observed in the equiaxed gamma grains located at lamellar

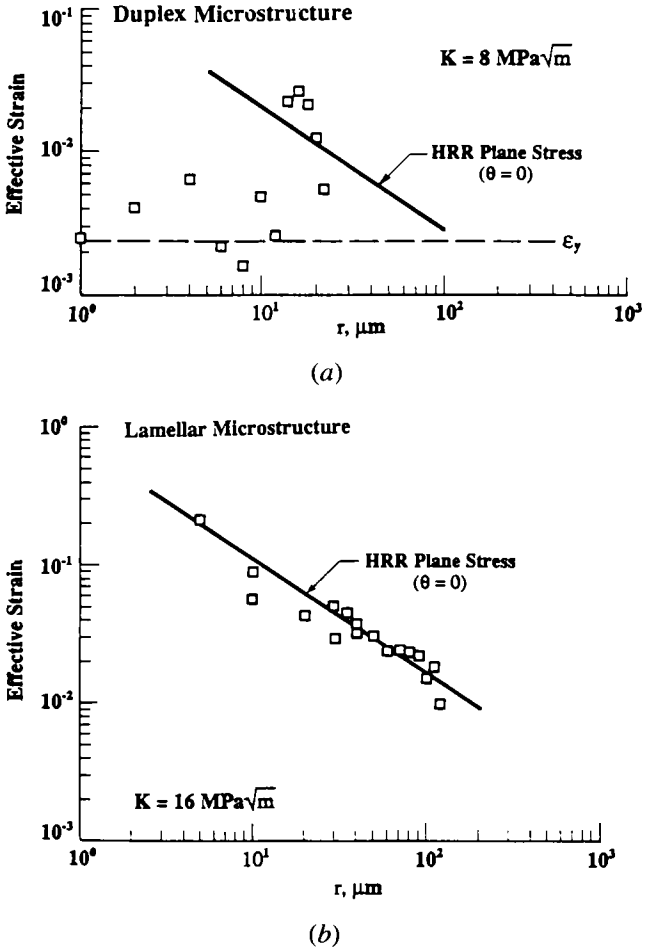

Fig. 10 — Measured near-tip strain distributions compared with the HRR field for plane stress: (*a*) duplex microstructure (G1F) and (*b*) near-lamellar microstructure (G1L).

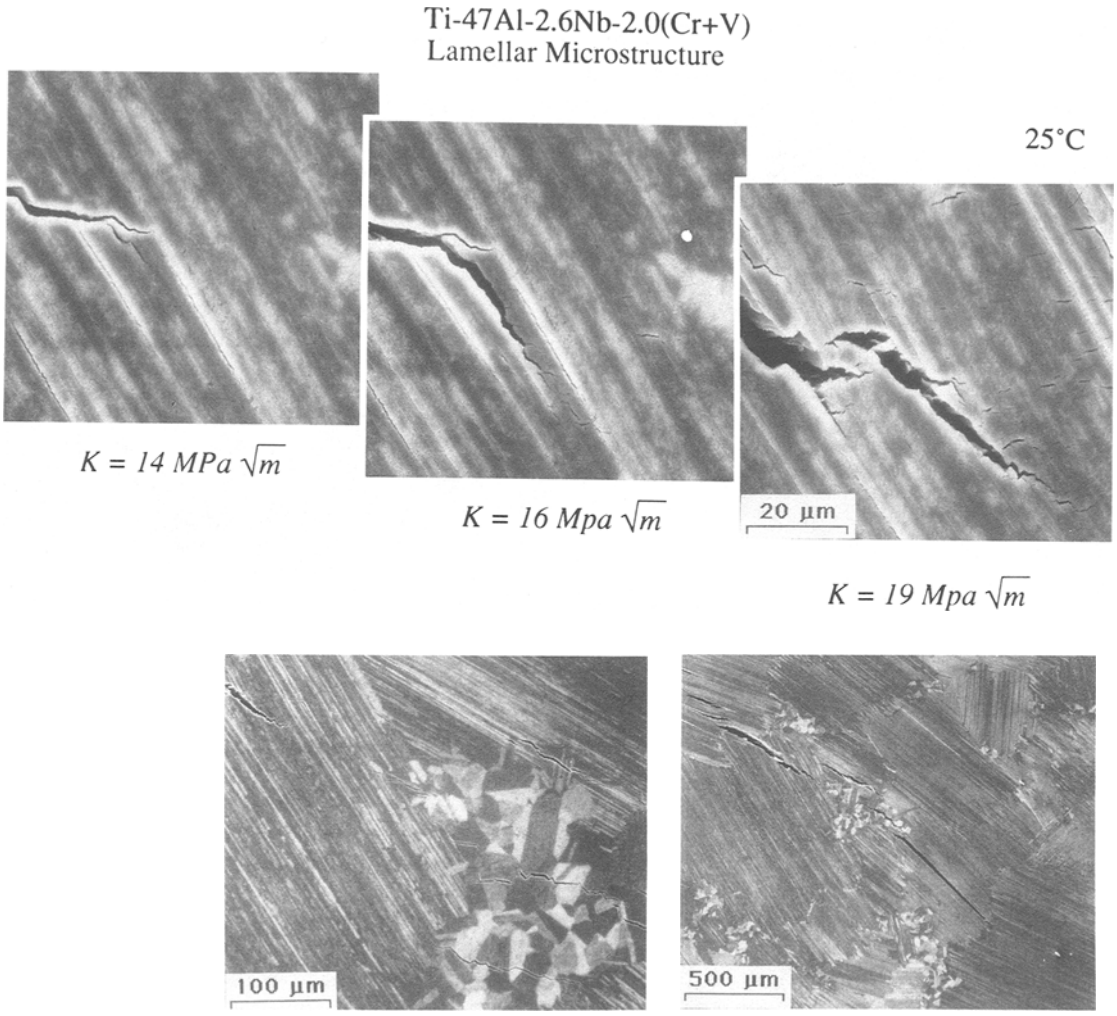

Fig. 11 — Near-tip fracture process in the near-lamellar microstructure (G1L) at 25 °C.

grain junctions. Initiation of microcracks in the equiaxed γ grains located at lamellar colony boundaries appeared to occur at $K = 20$ MPa$\sqrt{\text{m}}$. Additionally, a lamellar grain located ahead of the crack tip was found to delaminate along the α_2/γ interface, forming an interface crack that extended across the entire lamellar grain. At $K = 24$ MPa$\sqrt{\text{m}}$, the main crack began to link with the microcracks as fracture of the ligaments was imminent. The specimen failed at $K = 25$ MPa$\sqrt{\text{m}}$ after the ligaments failed. This led to a saturated value, K_s, in the K-resistance curve, as shown in Figure 8. The value of K_s was computed based on the crack length and the peak load at the onset of unstable fracture.

The fracture processes in the lamellar microstructure at 800 °C were quite similar to those at ambient temperature, but they occurred at higher K levels. Figure 12 illustrates the fracture processes associated with propagating the main crack across a lamellar colony. At $K = 9$ MPa$\sqrt{\text{m}}$, the main crack was seen to open. With increasing K levels, the lamellae ahead of the tip of the crack exhibited substantial amounts of plastic deformation, which resulted in bending of the platelets and formation of microcracks, as evidently shown at $K = 25$ MPa$\sqrt{\text{m}}$.

Another common fracture process at 800 °C was crack propagation in a direction parallel to α_2/γ lamellae, developing a shear band at the tip of the crack tip, as shown in Figure 13. Upon increasing K levels, the crack tip blunted by deforming along the shear band, and a microcrack was formed ahead of the tip of the main crack by delamination along an apparent interface. The interface crack and the main crack were, however, unconnected and separated by a shear ligament. Increasing the K level led to (1) intense deformation and fracture of the shear ligament, (2) opening of the microcrack, and (3) the development of a shear band at the tip of the interface microcrack. This combination of interface cracking and shear ligament fracturing process is clearly demonstrated in the series of micrographs for $K = 48$, 50, and 52 MPa$\sqrt{\text{m}}$ in Figure 13. From these micrographs, it is noted that the same crack extension process prevailed over the K range examined. The size of the shear ligaments and the amount of crack extension were, however, increased with increasing K levels.

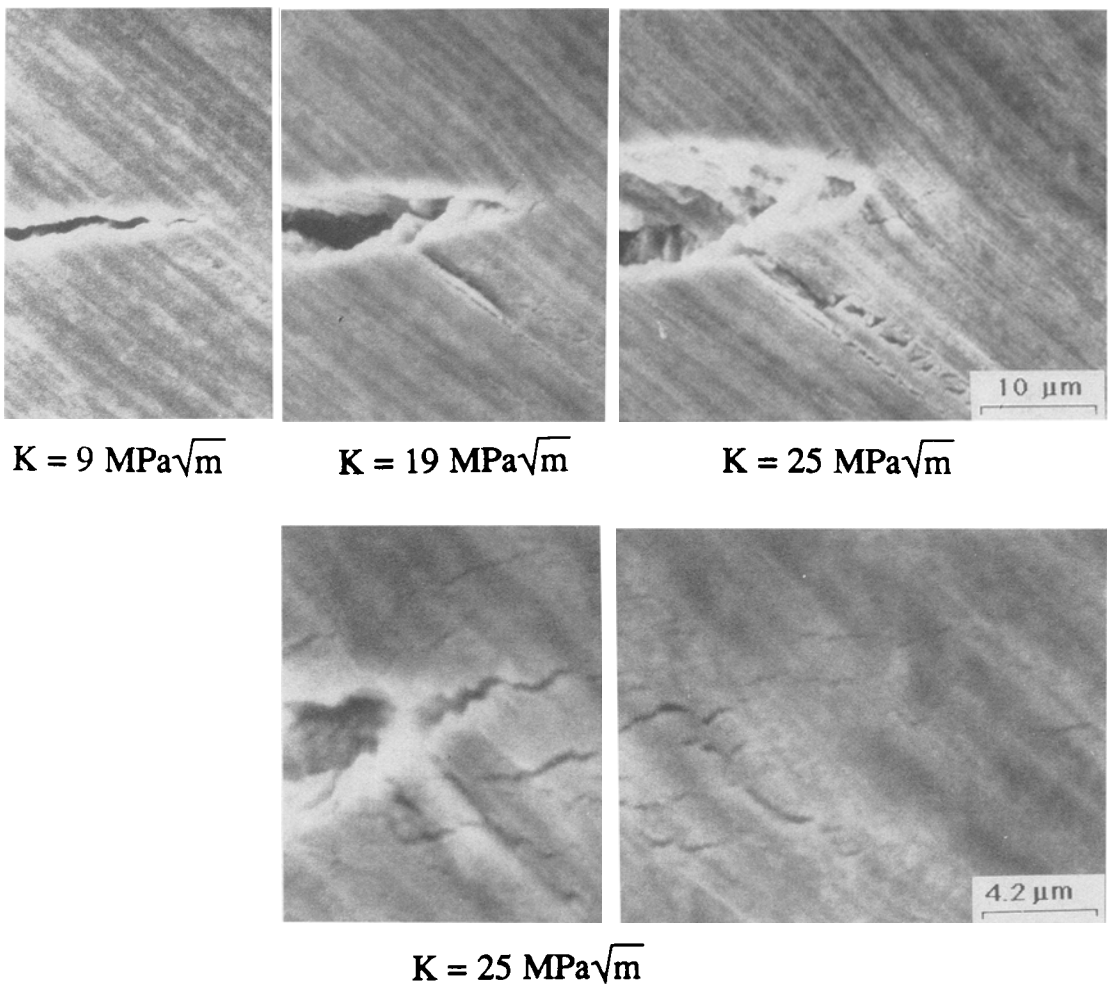

Fig. 12 — Fracture process associated with crack growth across the α_2/γ lamellae in the lamellar microstructure (G1L) at 800 °C.

The near-tip strain distributions for the cracks shown in Figures 12 and 13 are compared with those calculated based on the Hutchinson,[23] Rice, and Rosengren[24] (HRR) field for the plane stress condition in Figure 14 for K = 25 and 56.4 MPa$\sqrt{m}$. In both cases, the measured strains were lower than the calculated results, although the differences were reduced at the higher K level (56.4 MPa$\sqrt{m}$). This may indicate that the local stress intensity factor, K_{tip}, was lower than the applied stress intensity factor, K, based on the stipulation that the plane stress assumption was valid. Comparison of measured and calculated crack surface opening measurements, shown in Figure 14(b), indicated that the near-tip K value, K_{tip}, was 16 MPa$\sqrt{m}$, compared to the applied value of 25 MPa$\sqrt{m}$. Thus, the near-tip strain and crack opening displacement (COD) measurements indicated the presence of at least one shielding mechanism influencing the crack tip, prior to the onset of quasi-static crack growth.

C. *Fractographic Observations*

The fracture mechanisms revealed by fractographic studies of the fracture surfaces were similar to those observed on the specimen surface during *in situ* fracture testing. For the duplex microstructure (G1F), both cleavage and intergranular facets were observed.[15] The small amounts of equiaxed gamma grains in the G1L material failed in similar manners as those in the G1F material. In contrast, the lamellar grains in the G1L material exhibited translamellar fracture (across the lamellae) (Figure 15(a)), and delamination of interfaces resulting in apparent low-energy facets (Figure 15(b)) on the fracture surface. In many instances, translamellar crack propagation was accompanied with concurrent interface delamination (Figure 15(c)). The separation of interface cracks could be as large as 100 μm (Figure 15(c)), or as small as 5 μm or less (Figure 15(d)).

Comparison of fracture surfaces of tensile specimens of G1L tested in air is shown in Figures 16(a) and (c), respectively, while those for the fracture specimens tested in a vacuum are shown in Figures 16(b) and (d). Lamellar colonies that fractured by translamellar paths exhibited a composite fracture appearance, while those by interface delamination were generally manifested as low-energy facets with various degrees of smoothness. While many of these interface facets exhibited a

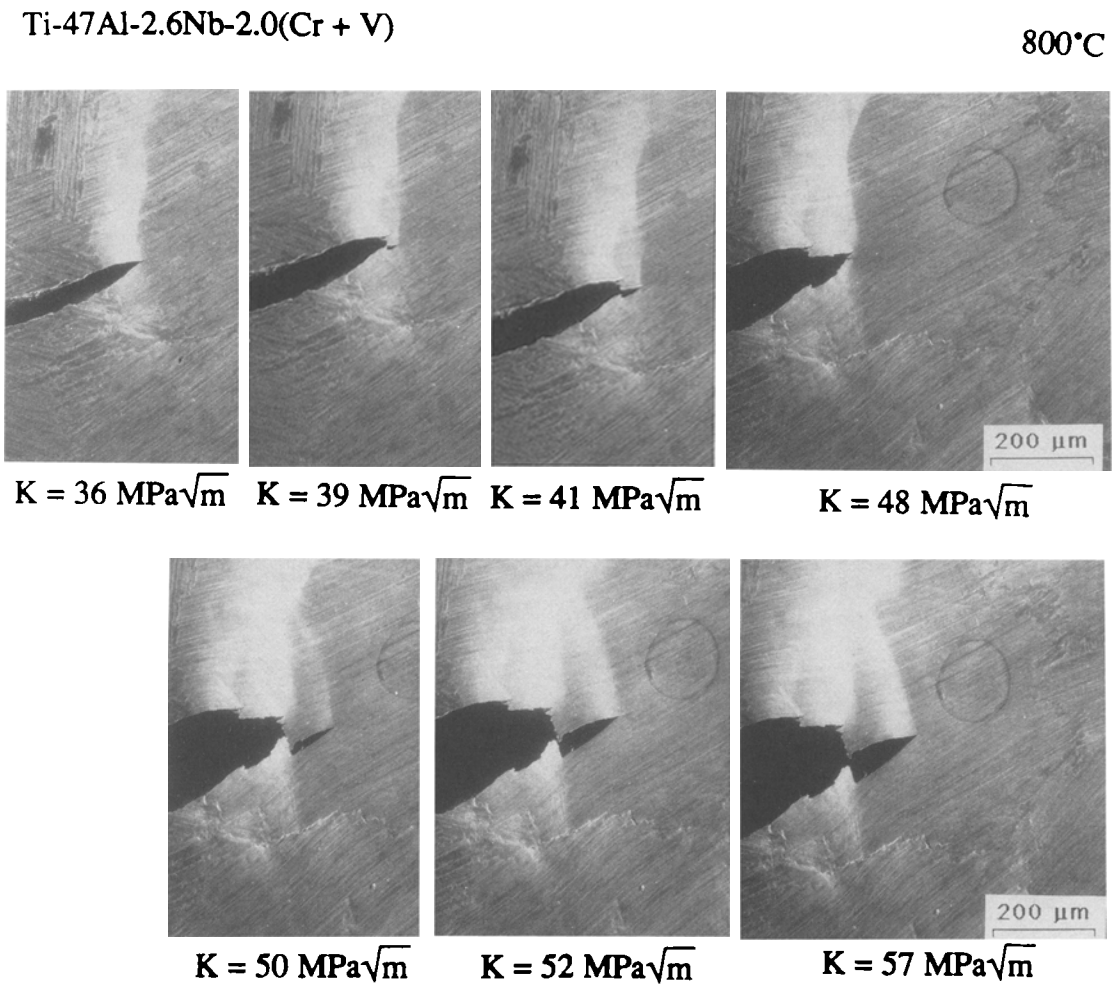

Fig. 13 — Fracture process associated with crack growth parallel to the α_2/γ interface in the lamellar microstructure (G1L) at 800 °C.

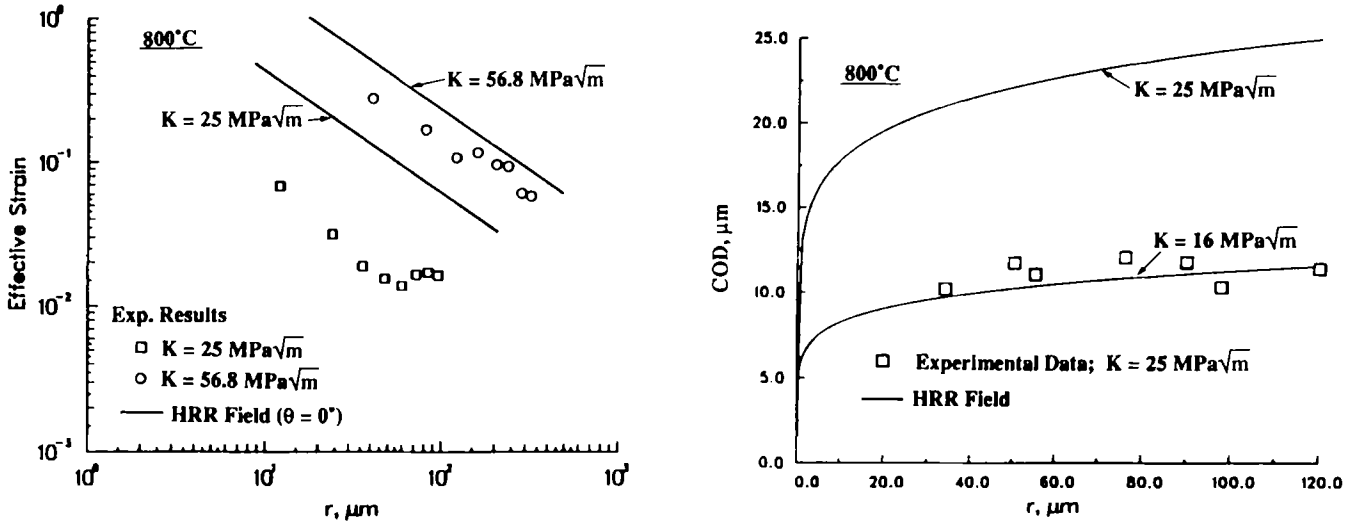

Fig. 14 — Comparison of measured near-tip strain distribution and CODs with the HRR field for plane stress for the lamellar material at 800 °C: (*a*) strain distribution and (*b*) COD.

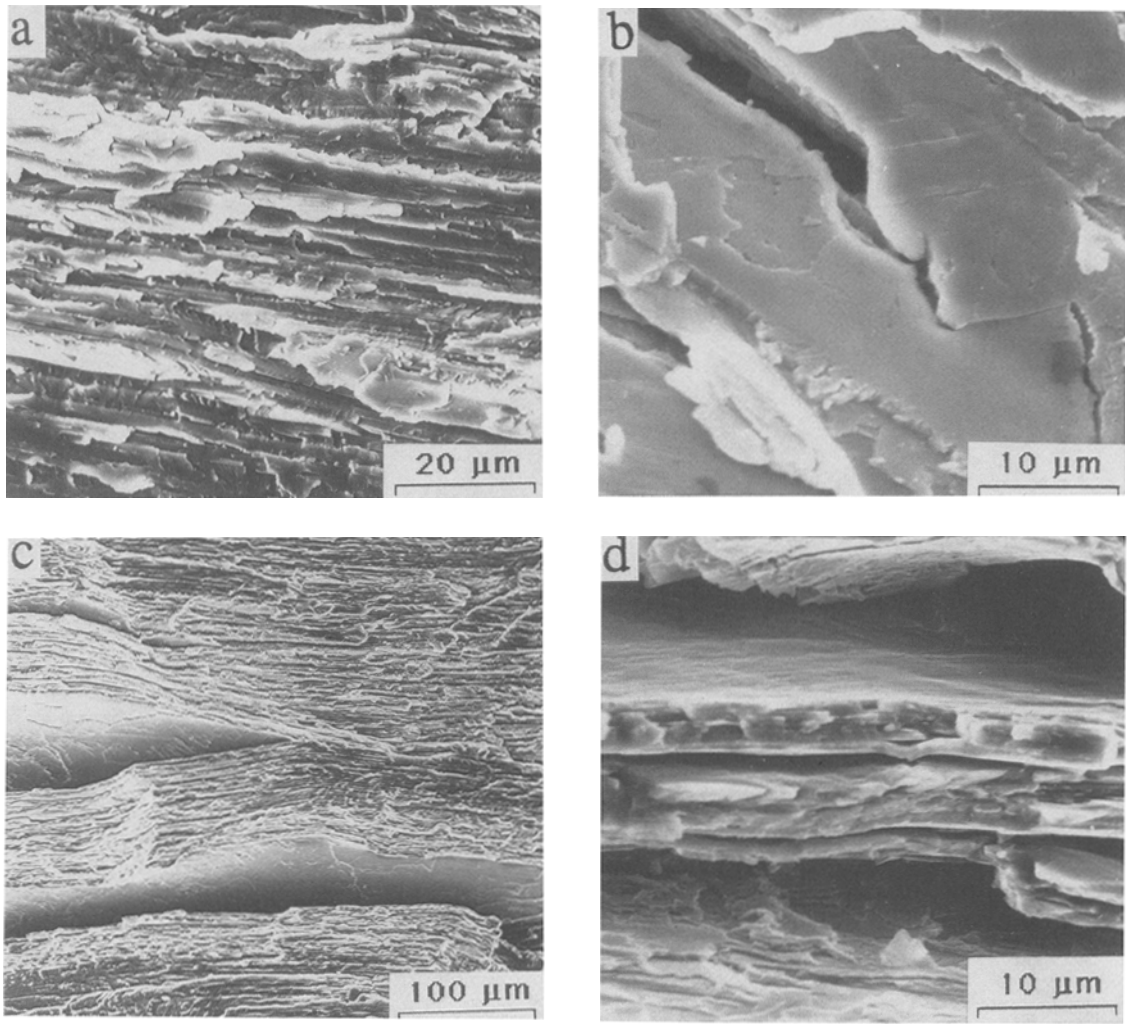

Fig. 15—Characteristics of fracture surfaces observed in the lamellar microstructure: (*a*) translamellar fracture, (*b*) interface facets, (*c*) translamellar fracture with concurrent interface delamination, and (*d*) high-magnification view of delaminated α_2/γ lamellae.

low-energy-like fracture appearance, there is evidence that delamination of these interfaces occurred with plastic dissipation resulting from both crack-tip blunting and fracture of shear ligaments (Figure 13). Figure 16 indicates the number of delamination facets on the fracture surfaces of G1L was quite large. Furthermore, interface delamination in the lamellar colonies occurred both in air and in vacuum at 25 °C and 800 °C. The available data are not sufficient to discern quantitatively whether interface delamination is assisted by the air environment or elevated temperature.

IV. DISCUSSION

The finding that the tensile ductility data in air and vacuum are equivalent at 25 °C in Figure 7(a) indicates that environment is not a factor affecting the tensile and fracture behavior of the lamellar microstructure at this temperature. The latter is confirmed by comparing the fracture toughness data obtained in this study to those obtained in air from another study.[6,17] Furthermore, the tensile ductility of the duplex microstructure was not influenced by the test environment at 600 °C. The different tensile and fracture toughness behaviors manifested by the duplex and the lamellar microstructures at ambient temperature are therefore of microstructural, and not of environmental, origins. On the other hand, the discrepancy between the tensile ductility in air and in vacuum at 800 °C suggested either an environmental degradation or a strain-rate effect associated with fracture of the lamellar material in air at elevated temperatures. The possible range of temperature and strain rate within which air might affect the fracture behaviors of the lamellar microstructure has not been investigated, however.

The tendency of the equiaxed gamma grain microstructure to exhibit grain boundary decohesion and cleavagelike fracture can be attributed to the planar slip behavior of the gamma grains. Because of the lack of five independent slip systems, planar slip in gamma grains would result in plastic incompatibility and, consequentially, microcrack formation at grain boundaries, as illustrated in Figure 17. In contrast, the lamellar microstructure exhibits a higher K_{IC} value than the equiaxed grain microstructure, despite lower total elongation and fracture strain. The higher K_{IC} value for the lamellar microstructure can be attributed directly to the

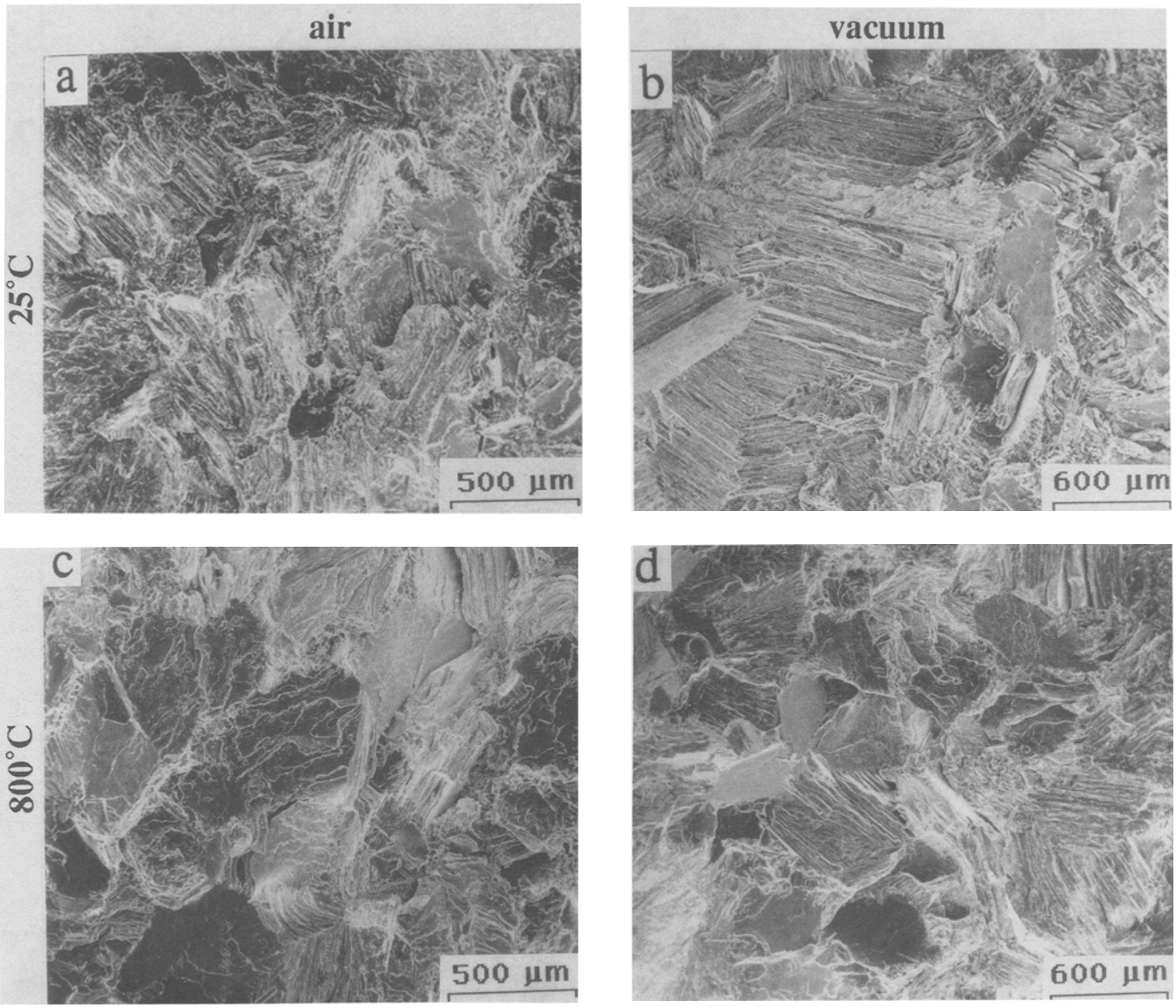

Fig. 16 — Comparison of fracture surfaces of tensile and fracture toughness specimens for G11. material: (*a*) tensile specimens at 25 °C in air, (*b*) fracture toughness specimens at 25 °C in vacuum, (*c*) tensile specimens at 800 °C in air, and (*d*) fracture toughness specimens at 800 °C in vacuum.

ability of the lamellar microstructure to sustain a higher plastic strain near the crack tip (Figure 17), without causing grain boundary decohesion or slipband cracking. The lamellar microstructure, however, has a tendency to delaminate along interfaces, producing relatively smooth and low-energy-like facets. Recent work[26] has identified the delaminated interfaces in the lamellar colonies to include γ/γ, γ/α_2, and α_2/α_2 interfaces. The results have been obtained by identifying the phases lying on top of the mating fracture surfaces using the energy-dispersive spectroscopy technique. The majority of the delaminated interfaces observed at ambient temperature are γ/γ interfaces, with the γ/α_2 interfaces less frequently observed. The α_2/α_2 interface was observed once at 800 °C.

At ambient temperature, the near-tip strain values for the lamellar microstructure are considerably larger than the tensile ductility measured in air or vacuum. Furthermore, the tensile ductility and K_{IC} values of the duplex and lamellar microstructures appear to correlate in an inverse manner. As shown in Table I, high values of K_{IC} and K_s correspond to lower tensile ductility and *vice versa*. The lack of correlation between K_{IC} and tensile ductility, which has been observed previously in α_2 titanium aluminide alloys[4,18] as well as TiAl-based alloys,[3,6,17] can be understood on the basis that the tensile ductility of the intermetallic alloy is likely to be dictated by the nucleation of a microcrack, whose length at initiation is greater than that required to attain the K_{IC} or J_{IC} under the imposed stress and strain conditions. Under this circumstance, the tensile ductility is dictated by the J_{IC} or K_{IC} value and the length of the microcrack, which is the gamma grain size in the duplex microstructure but is the colony size in the lamellar microstructure. Using a previous model by Chan,[27] which describes this type of fracture process, the tensile ductilities of both equiaxed

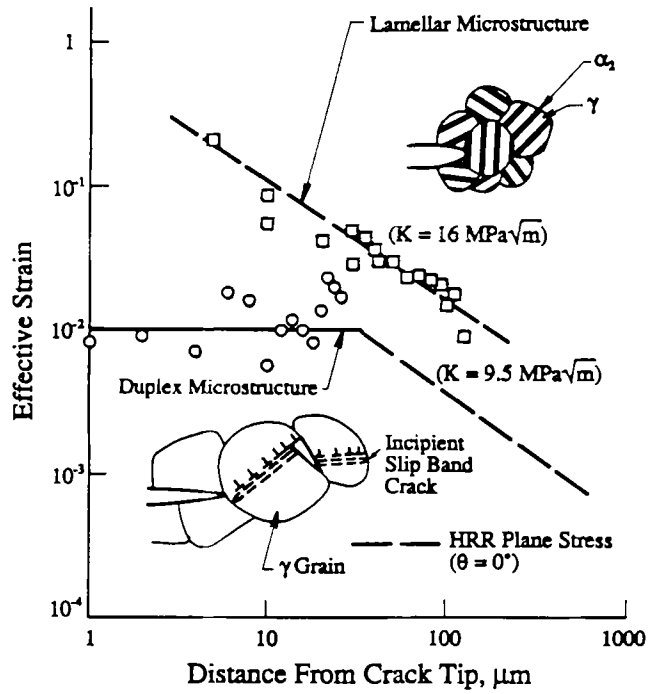

Fig. 17—Comparison of near-tip fracture process and strain distribution in the duplex (GTF) and the lamellar (GTL) microstructures for 25 °C.

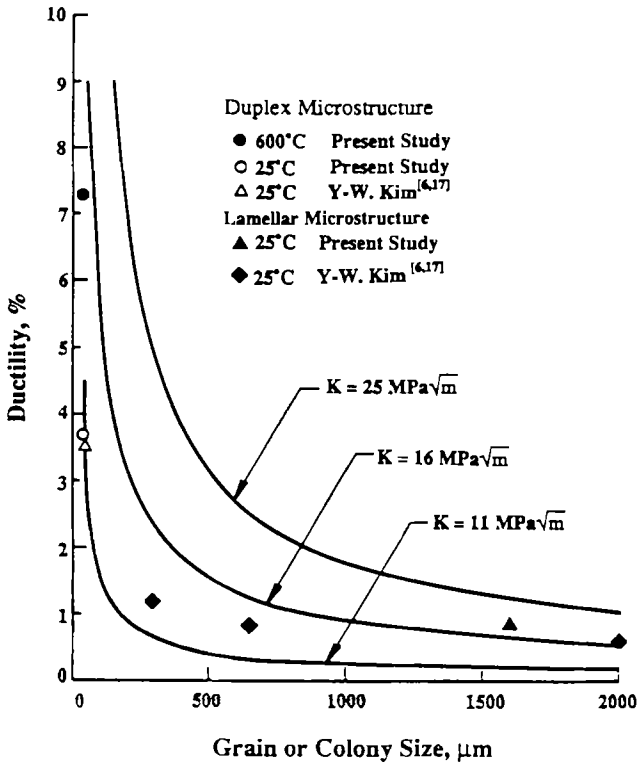

Fig. 18—Comparison of observed and calculated tensile ductility as a function of grain or colony size for TiAl-alloys.

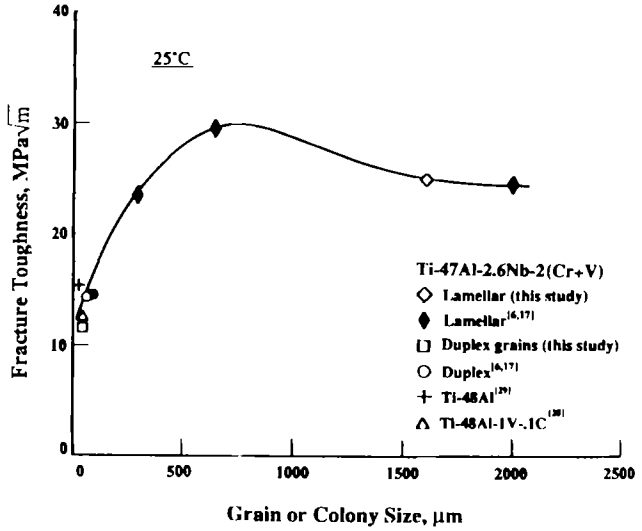

Fig. 19—Dependence of fracture toughness (K_s) on grain or colony size for TiAl-alloys.

and lamellar microstructures have been calculated using Eqs. (1) through (7) in Reference 27, and the results are presented in Figure 18. In these calculations, a microcrack length equal to the grain or colony size was assumed to be present in the microstructure. A grain boundary microcrack was assumed in the duplex microstructure, while an interface crack formed by delamination of the α_2/γ colony was envisioned in the lamellar microstructure. The fracture strain values corresponding to K_{IC} and K_s are both presented. The important point to note in Figure 18 is that the low tensile ductility in the lamellar microstructure is the result of the relatively large colony size. Conversely, the higher tensile ductility observed in the equiaxed microstructure is due to a small grain size.

Another important difference between the duplex and the lamellar microstructures is in the tearing resistance. In particular, the duplex microstructure exhibits no tearing resistance ($T_R = 0$) at 25 °C and 600 °C. In contrast, the lamellar microstructure shows moderate and outstanding tearing resistance at 25 °C and 800 °C, respectively. The resistance-curve behavior exhibited by the lamellar microstructure at 25 °C appears to arise from the tendency of the main crack to change crack paths as it zigzags among individual colonies, resulting in mismatched crack planes that are connected by unbroken ligaments. Fracture of these ligaments, which generally occurs in shear (Figures 8 and 13), requires additional plastic dissipation that can lead to toughness enhancement. A recent analysis by Chan[25] has revealed that shear ligament toughening leads to a resistance-curve behavior similar to bridging of the crack surfaces. The amount of toughness enhancement increases with increasing area fraction and fracture toughness (plastic work of fracture) of the shear ligaments on the crack plane, as well as the size of the lamellar colony. Figure 19 shows comparison of the fracture toughness of several TiAl-alloys, both from this and other studies.[6,17,28,29] The fracture toughness data in this plot are the maximum values of intensity, K_s, measured at the peak load. Therefore, they include both

the initiation toughness (K_{IC}) and the resistance-curve effect. The comparison shows that the lamellar microstructure exhibits a higher toughness than materials with the equiaxed gamma grain or duplex microstructures. For the lamellar microstructure in this study, the K_{IC} values at which stable and unstable crack growth occurs are 16 and 25 MPa$\sqrt{m}$, respectively. The toughening ratio (K_S/K_{IC}), which can be attributed to shear ligament toughening, is 1.56. The toughness enhancement, presumably due to shear ligament toughening, appears to reach a maximum at a colony size of 600 μm. From Figures 18 and 19, it is also evident that tensile ductility and fracture toughness depend on colony or grain size in opposite manners. As a result, tensile ductility and fracture toughness are not expected to correlate through a simple relationship, as observed experimentally.

The sources of tensile ductility and fracture toughness in the lamellar microstructure at 800 °C are not readily obvious based on the results obtained in this investigation. Although shear ligament toughness has been identified as one of the toughening mechanisms, near-tip strain measurements and plastic bending of the lamellae ahead of the crack tip clearly indicate ductility in this microstructure at 800 °C, at least in the vacuum environment and at slow strain rate. Subsequent transmission electron microscopy studies[26,30] of deformed tensile specimens have revealed the presence of twins in the γ platelets in the lamellar microstructure at both 25 °C and 800 °C. The amount of twins and dislocations is considerably higher in specimens tested at 800 °C than at 25 °C. This finding suggests that the improved tensile ductility and fracture toughness characteristics of the lamellar microstructure at 800 °C are the consequence of the activation of additional twinning or slip systems, at least in the γ phase.

The near-tip strain distribution in the lamellar microstructure has been found to be the HRR-type[23,24] (power-law type) for the plane stress condition when the cracks are stationary or exhibit small crack extensions. This conclusion is based on near-tip strain distributions for θ = 0 deg, 45 deg, and 90 deg, although only those results for θ = 0 deg are shown in Figures 10 and 14. The finding is in agreement with previous results for quasi-static crack growth in Al-Fe-X alloys[31] and Ti-24Al-11Nb.[18,25] Furthermore, it is consistent with recent near-tip in-plane displacement measurements obtained *via* a moire interferometry by Dadkhah and Kobayashi[32] which showed the dominance of the plane-stress HRR-field for dynamic cracks with less than 2 to 10-mm crack increments. In all cases, the loss of HRR dominance was observed only after substantial crack extensions had occurred. For elastic-plastic stationary cracks, finite-element analyses[32] revealed that the plane stress assumption is valid at the surfaces of a thin sheet specimen for distances as close as one crack-tip opening displacement from the crack tip. Since only in-plane strain components were measured in this investigation, possible breakdown of the plane stress assumption due to three-dimensional surface effects[33,34] cannot be deduced from the strain measurements. The resolution of the machine-vision-based stereoimaging technique is better than 1 μm in displacement and 0.5 pct in strain. As a result, the discrepancies between measured and calculated near-tip strains and CODs shown in Figures 10 and 14 are not the consequence of experimental limitation. Instead, they are apparently due to the intervention of microcrack nucleation at a grain boundary (Figure 9) and the presence of shielding mechanisms that reduce the near-tip stress intensity factor (Figure 14). The colony size of the lamellar microstructure of the alloy studied is ≈1.6 mm. Because of this relatively large colony size, there is a concern about the use of the HRR theory at a smaller size scale. Nonetheless, the measured strains exhibited the HRR-type distribution. This behavior can be attributed to the fact that plastic deformation within the lamellar colony is controlled not by the colony size but by the spacing of the lamellae, which is on the order of 1 μm for this alloy.

V. CONCLUSIONS

1. The fracture mechanisms in the duplex microstructure are plasticity-induced grain boundary decohesion and cleavage, while those in the lamellar microstructure are interface delamination and cracking across the lamellae.
2. The lamellar microstructure is tougher than the equiaxed gamma or duplex microstructure because of higher near-tip plasticity and an anisotropic compositelike fracture characteristic that yields a tortuous crack path, shear ligament toughening, and an improved resistance-curve behavior.
3. Tensile ductility of the lamellar microstructure increases with decreasing colony size, while fracture toughness shows a maximum at a large colony size. There is no correlation between fracture toughness (K_{IC} values) and measured tensile ductility in the two-phase TiAl alloy. The lack of a correlation is the consequence of an opposite dependence of tensile ductility and fracture toughness on grain or colony size.
4. Tensile ductility of the lamellar microstructure at 800 °C is adversely affected by a slow strain rate in the air environment.

ACKNOWLEDGEMENTS

The contributions of K.S. Chan and Y.-W. Kim were supported, respectively, by the Air Force Office of Scientific Research, through Contract No. F49620-89-C-0032, and the Air Force Materials Lab, through Contract No. F33615-89-C-5629. K.S. Chan is thankful for the encouragement and support provided by the Program Manager, Dr. Alan Rosenstein. The technical assistance of Mr. J. Campbell and Mr. J. Spencer, the editorial assistance of Ms. D. Stowitts, and the clerical assistance of Ms. J. McCombs of Southwest Research Institute, San Antonio, TX, are acknowledged. The technical assistance by S. Boone, Metcut-Materials Research Group, Wright-Patterson Air Force Base, OH, is also acknowledged.

REFERENCES

1. Y.-W. Kim: *J. Met.*, 1989, vol. 41 (7), pp. 24-30.
2. Y.-W. Kim and F.H. Froes: in *High-Temperature Aluminides and*

Intermetallics, S.H. Whang, C.T. Liu, D. Pope, and J.O. Stiegler, eds., *TMS*, Warrendale, PA, 1990, pp. 465-92.
3. Y.-W. Kim: in *High Temperature Ordered Intermetallic Alloys IV*, J.O. Stiegler, L.A. Johnson, and D.P. Pope, eds., MRS, Pittsburgh, PA, 1991, pp. 777-94.
4. J.M. Larsen, K.A. Williams, S.J. Balsone, and M.A. Stucke: in *High-Temperature Aluminides and Intermetallics*, S.H. Whang, C.T. Liu, D. Pope, and J.O. Stiegler, eds., *TMS*, Warrendale, PA, 1990, pp. 521-56.
5. Y.-W. Kim: in *Intermetallic Compounds-Structure and Mechanical Properties-JIMIS 6*, O. Izumi, ed., Japan Institute of Metals, Sendai, Japan, 1991, pp. 753-62.
6. Y.-W. Kim: *Acta Metall.*, in press.
7. S.-C. Huang and E.L. Hall: in *High-Temperature Ordered Intermetallic Alloys III*, C.T. Liu, A.J. Taub, N.S. Stoloff, and C.C. Koch, eds., *MRS*, Pittsburgh, PA, 1989, vol. 133, pp. 373-83.
8. T. Tsujimoto and K. Hashimoto: in *High-Temperature Ordered Intermetallic Alloys III*, C.T. Liu, A.J. Taub, N.S. Stoloff, and C.C. Koch, eds., *MRS*, Pittsburgh, PA, 1989, vol. 133, pp. 391-96.
9. T. Kawabata, T. Tamura, and O. Izumi: in *High-Temperature Ordered Intermetallic Alloys III*, C.T. Liu, A.J. Taub, N.S. Stoloff, and C.C. Koch, eds., *MRS*, Pittsburgh, Pa, 1989, vol. 133, pp. 329-34.
10. Y.-W. Kim and D.M. Dimiduk: *J. Met.*, 1991, vol. 43 (8), pp. 40-47.
11. J.J. Valencia, C. McCullough, C.G. Levi, and R. Mehrabian: *Scripta Metall.*, 1987, vol. 21, pp. 1341-46.
12. D.S. Shong and Y.-W. Kim: *Scripta Metall.*, 1989, vol. 23, pp. 257-61.
13. Y.-W. Kim and J.J. Kleek: *PM 90—World Conference on Powder Metallurgy*, The Institute of Metals, London, 1990, vol. 1, pp. 272-88.
14. M.J. Blackburn and M.P. Smith: AFWAL Technical Report No. AFWAL-TR-82-4086, 1982.
15. K.S. Chan and Y.-W. Kim: in *Microstructure/Property Relationships in Titanium Alloys and Titanium Aluminides*, Y.-W. Kim and R.R. Boyer, eds., *TMS*, Warrendale, PA, 1991, pp. 179-96.
16. P.G. Breig and S.W. Scoot: *Materials and Manufacturing Processes*, 1989, vol. 4 (1), pp. 77-83.
17. Y.-W. Kim: in *Microstructure/Property Relationships in Titanium Alloys and Titanium Aluminides*, Y.-W. Kim and R.R. Boyer, eds., *TMS*, Warrendale, PA, 1991, pp. 91-103.
18. K.S. Chan: *Metall. Trans. A*, 1990, vol. 21A, pp. 2687-99.
19. A. Nagy, J.B. Campbell, and D.L. Davidson: *Rev. Sci. Instrum.*, 1984, vol. 55, pp. 778-82.
20. E.A. Franke, D.J. Wenzel, and D.L. Davidson: *Rev. Sci. Instrum.*, 1990, vol. 62 (5), pp. 1270-79.
21. D.L. Davidson, K.S. Chan, and R.A. Page: in *Micromechanics: Experimental Techniques*, W. Sharpe, ed., *ASME*, New York, NY, 1989, AMD-vol. 102, pp. 73-87.
22. D.R. Williams, D.L. Davidson, and J. Lankford: *Experimental Mechanics*, 1980, vol. 20, pp. 134-39.
23. J.W. Hutchinson: *J. Mech. Phys. Solids*, 1968, vol. 16, pp. 13-31.
24. J.R. Rice and G.R. Rosengren: *J. Mech. Phys. Solids*, 1968, vol. 16, pp. 1-13.
25. K.S. Chan: *Metall. Trans. A*, 1991, vol. 22A, pp. 2021-29.
26. K.S. Chan and Y.-W. Kim: *Metall. Trans. A*, in press.
27. K.S. Chan: *Scripta Metall.*, 1990, vol. 24, pp. 1725-30.
28. M.J. Blackburn and M.P. Smith: AFWAL Technical Report No. AFWAL-TR-82-4086, 1982.
29. W.O. Soboyejo, S.J. Midea, D.S. Schwartz, and M.J. Parzuchowski: in *Microstructure/Property Relationships in Titanium Alloys and Titanium Aluminides*, Y.-W. Kim, R.R. Boyer, and J.A. Hall, eds., *TMS*, Warrendale, PA, 1991, pp. 197-212.
30. Y. Pan: Southwest Research Institute, San Antonio, TX, unpublished research, 1991.
31. K.S. Chan: *Metall. Trans.*, 1990, vol. 21A, pp. 69-80.
32. M.S. Dadkhah and A.S. Kobayashi: *Eng. Fract. Mech.*, 1989, vol. 34, pp. 253-62.
33. C.L. Hom and R.M. McMeeking: in *Analytical, Numerical, and Experimental Aspects of Three-Dimensional Fracture Processes*, A.J. Rosakis, K. Ravi-Chandar, and Y. Rajapakse, eds., ASME, New York, NY, 1988, AMD-vol. 91, pp. 215-26.
34. T. Nakamura and D.M. Parks: in *Analytical, Numerical, and Experimental Aspects of Three-Dimensional Fracture Processes*, A.J. Rosakis, K. Ravi-Chandar, and Y. Rajapakse, eds., ASME, New York, NY, 1988, AMD-vol. 91, pp. 215-26.